Pixatimod (PG545), a clinical-stage heparan sulfate mimetic, is a potent inhibitor of the SARS-CoV-2 virus

Scott E. Guimond[1,*], Courtney J. Mycroft-West[1,*], Neha S. Gandhi[2,*], Julia A Tree[3,*], Karen R Buttigieg[3], Naomi Coombes[3], Kristina Nystrom[4], Joanna Said[4], Yin Xiang Setoh[5,6], Alberto Amarilla[5,6], Naphak Modhiran[5,6], De Jun Julian Sng[5,6], Mohit Chhabra[5,6], Daniel Watterson[5,6] , Paul R Young[5,6], Alexander A Khromykh[5,6], Marcelo A. Lima[1], David G Fernig[7], Dunhao Su[7], Edwin A.Yates[7], Edward Hammond[8], Keith Dredge[8], Miles W Carroll[3,$], Edward Trybala[4,$], Tomas Bergstrom[4,$], Vito Ferro,[5,6,$] Mark A. Skidmore[1,$] and Jeremy E Turnbull[7,9$]

[1]Molecular & Structural Biosciences, School of Life Sciences, Keele University, Newcastle-Under-Lyme, Staffordshire, ST5 5BG, UK.
[2]School of Mathematical Sciences and Institute of Health and Biomedical Innovation, Queensland University of Technology, 2 George Street, Brisbane, QLD 4000, Australia.
[3]National Infection Service, Public Health England, Porton Down, Salisbury, Wiltshire, England, UK, SP5 3NU.
[4]Department of Infectious Diseases, Institute of Biomedicine, University of Gothenburg, Guldhedsgatan 10B, S-413 46 Goteborg, Sweden
[5]School of Chemistry and Molecular Biosciences, the University of Queensland, Brisbane, QLD 4072, Australia;
[6]Australian Infectious Diseases Research Centre, the University of Queensland, Brisbane, QLD 4072, Australia
[7]Department of Biochemistry and Systems Biology, Institute of Systems, Molecular and Integrative Biology, University of Liverpool, Liverpool, L69 7ZB, UK
[8]Zucero Therapeutics Ltd, 1 Westlink Court, Brisbane, Queensland 4076, Australia.
[9]Copenhagen Center for Glycomics, Department of Cellular & Molecular Medicine, University of Copenhagen, Copenhagen N 2200, Denmark

*These authors contributed equally
[$]Equal senior authors
Corresponding author: j.turnbull@liverpool.ac.uk; +44 (0)151 795 4427

Keywords

Pixatimod, PG545, heparan sulfate, SARS-CoV-2, COVID-19, heparan sulfate mimetic, antiviral, heparanase inhibitor

Abstract

A major global effort is currently ongoing to search for therapeutics and vaccines to treat or prevent infection by the SARS-CoV-2 virus. Repurposing existing entities is one attractive approach. The heparan sulfate mimetic pixatimod is a clinical-stage synthetic sulfated compound that is a potent inhibitor of the glycosidase heparanase, and has known anti-cancer, anti-inflammatory and also antiviral properties. Here we show that pixatimod binds directly to the SARS-CoV-2 spike protein S1 receptor binding domain (RBD) and alters its conformation. Notably, this site overlaps with the known ACE2 binding site in the S1 RBD. We find that pixatimod inhibits binding of recombinant S1 RBD to Vero cells which express the ACE2 receptor. Moreover, in assays with three different isolates of live SARS-CoV-2 virus we show that pixatimod effectively inhibits viral infection of Vero cells. Importantly, its potency is well within its safe therapeutic dose range. These data provide evidence that pixatimod is a potent antiviral agent against SARS-CoV-2. Together with its other known activities this provides a strong rationale for its clinical investigation as a new multimodal therapeutic for the current COVID-19 pandemic.

Introduction

The coronavirus-19 disease (COVID-19) pandemic caused by the severe acute respiratory syndrome coronavirus 2 (SARS-CoV-2) is approaching nine million cases world-wide (8,860,331 as of 22nd June 2020), causing more than 465,740 deaths [WHO 2020]. The disease progression over time is divided into three pathological phases: an early infection phase, a pulmonary phase, and a severe hyper-inflammation phase (Akhmerov et al, 2020). Unlike other coronaviruses, it is now evident that SARS-CoV-2 has the ability to infect lung epithelium, gut enterocytes and endothelial cells (Lamers et al, 2020; Varga et al, 2020; Yao et al, 2020; Ackermann et al, 2020). Thus, the SARS-CoV-2 virus has the potential to cause not only the viral pneumonia that progresses to acute respiratory distress syndrome (ARDS, Guan et al, 2020), but also other complications such as cardiac injury (Akhmerov et al, 2020), acute kidney injury (Chan et al, 2020) and even multi-organ failure (Renu et al, 2020). Given the severe pathophysiology induced by COVID-19, the need for therapeutic alternatives to alleviate and stop this epidemic is clear (Martinez et al, 2020).

Heparan sulfate (HS) is a highly sulfated glycosaminoglycan found on the surface of most mammalian cells (Li et al, 2016) which is used by many viruses as an entry receptor or co-receptor (Cagno et al, 2019), including coronaviruses (Milewska et al, 2014; Lang et al, 2011). Various compounds that mimic HS, e.g., heparin and other sulfated polysaccharides, have been extensively investigated and have been shown to block infectivity and cell-to-cell spread in a multitude of different viruses, including SARS-associated coronavirus strain HSR1 (Vicenzi et al, 2004). The glycosylated spike (S) protein of SARS-CoV-2 mediates host cell invasion via binding to a receptor protein, angiotensin-converting enzyme 2 (ACE2, Hoffmann et al, 2020; Wrapp et al, 2020). Analysis of the sequence and experimentally determined structures of the S protein (Wrapp et al, 2020; Shang et al, 2020; Lan et al, 2020) reveals that the receptor binding domain (RBD) of the S1 subunit contains a HS binding site. Recent studies have clearly demonstrated binding of heparin and HS to S1 RBD (Mycroft-West, 2020a; Mycroft-West, 2020b; Mycroft-West, 2020c; Liu, 2020), including induction of significant conformational change in the S1 RBD structure (Mycroft-West et al, 2020a). These data strongly suggest that SARS-CoV-2 is dependent upon HS-binding for host cell entry and that blocking this process with HS mimetics has potential as an effective strategy for COVID-19 therapy.

Pixatimod (PG545) is a clinical-stage HS mimetic with potent anti-cancer (Dredge et al, 2011; Ferro et al, 2012), and anti-inflammatory properties (Khamaysi et al, 2017; Abassi et al, 2017; Koliesnik et al, 2020), but also antiviral activities (Said et al, 2010; Lundin et al, 2012; Said et al, 2016; Supramaniam et al, 2018;

Modhiran et al, 2019). Significant antiviral activity for pixatimod has been reported against a number of viruses that use HS as an entry receptor with EC_{50}'s ranging from 0.06 to 14 µg/mL. This includes HSV-2 (Said et al, 2016), HIV (Said et al, 2010), RSV (Lundin et al, 2012), Ross River, Barmah Forest, Asian CHIK and chikungunya viruses (Supramaniam et al, 2018), and Dengue virus (Modhiran et al, 2019). In addition to blocking virus infectivity, pixatimod has also been shown to possess virucidal activity, a unique feature only found in this particular class of amphiphilic HS mimetic (Ekblad et al, 2010; Said et al, 2016). The virucidal activity is due to disruption of the viral lipid envelope by the lipophilic steroid side chain of pixatimod (see **Fig 1A**), an attribute not associated with heparin or other HS mimetics (Said et al, 2016). *In vivo* efficacy has been confirmed in a prophylactic mouse HSV-2 genital infection model (Said et al, 2016), a prophylactic Ross River virus mouse model (Supramaniam et al, 2018) and a therapeutic Dengue virus mouse model (Modhiran et al, 2019).

Pixatimod has been evaluated in a Phase Ia clinical trial in patients with advanced solid tumours where it demonstrated a tolerable safety profile and some evidence of disease control (Dredge et al, 2018; Hammond et al, 2018). It is currently undergoing a Phase Ib study in combination with nivolumab in patients with pancreatic or bowel cancers (Kuo et al, 2018). Given pixatimod has been safely administered to 80 patients (unpublished data) and that its HS-mimetic activity shows potential to inhibit the SARS-CoV-2 virus, it was tested for anti-viral activity against this virus with the aim to progress into clinical trials against COVID-19.

Here we provide evidence of a direct interaction of pixatimod with the S1 spike protein RBD, supported by molecular modelling data. Pixatimod was also able to inhibit the interaction of S1-RBD with Vero cells which are known to express the ACE2 receptor. Finally we established that pixatimod is a potent inhibitor of attachment and invasion of Vero cells by live SARS-CoV-2 virus, and reduces its cytopathic effect, at concentrations within the known therapeutic range of this drug. Our data provide strong support for clinical investigation of the potential of pixatimod as a novel therapeutic intervention for prophylaxis and treatment of COVID-19.

Results

Molecular modelling of interactions of pixatimod with the spike protein S1 receptor binding domain

We initially used molecular dynamics (MD) simulations to map the potential binding sites of pixatimod (**Fig 1A**) on the S1 RBD surface (**Fig 1B**). A total of 24 unique residues of RBD were identified to be interacting with several residues of ACE based on the X-ray structures (**Fig 1B**). Amino acids making significant interactions with pixatimod were identified on the basis of their individual contributions to the total interaction energy, considering only the residues that contribute less than -1.0 kcal/mol and a number of these residues (Tyr489, Phe456, Leu455, Ala475) are also involved in binding to ACE2. The decomposition approach was helpful for locating residues of the RBD domain such as Lys458, Ser459, Lys462 and Asn481, that transiently interact to form hydrogen bonds or ionic interactions with the sulfated tetrasaccharide of pixatimod (**Fig S1**). The free energy of binding is -10 kcal/mol, wherein van der Waals energies have the major favourable contribution to the total free energy. The cholestanol residue formed stabilizing interactions with Tyr489, Phe456, Tyr473, Ala475, Gln474 and Leu455 (**Fig S1**). Furthermore, the standard deviation of backbone RMSD around residues Leu455-Pro491 and the N-terminal of RBD (Thr333-Thr345) among the four repeated MD trajectories were approximately 2Å, indicating significant conformational change in the region. RMSF calculations of main-chain atoms showed significant atomic fluctuations (≥1.5 Å) for Lys458, Asn460, Lys462, Arg466, Ser477 and Asn481 upon

binding to the ligand pixatimod. These results indicate that a conformational change may be induced by binding of pixatimod to S1 RBD (**Fig 1C**).

An alternate heparin binding site is reported around residues Arg403, Arg406, Arg408, Gln409, Lys417, Gln493, Gln498 (Mycroft-West et al, 2020c). One of the replicates indicated a second binding mode wherein the tetrasaccharide of pixatimod was found to interact around this region (**Fig S2**), however, the free energy of binding was > +13 kcal/mol indicating much less favourable binding to this site.

Overall, our modelling data strongly support the notion of direct binding of pixatimod to S1 RBD, potentially resulting in induction of a conformational change. Furthermore, the data also suggested that pixatimod could potentially interfere with binding of S1 RBD to ACE2.

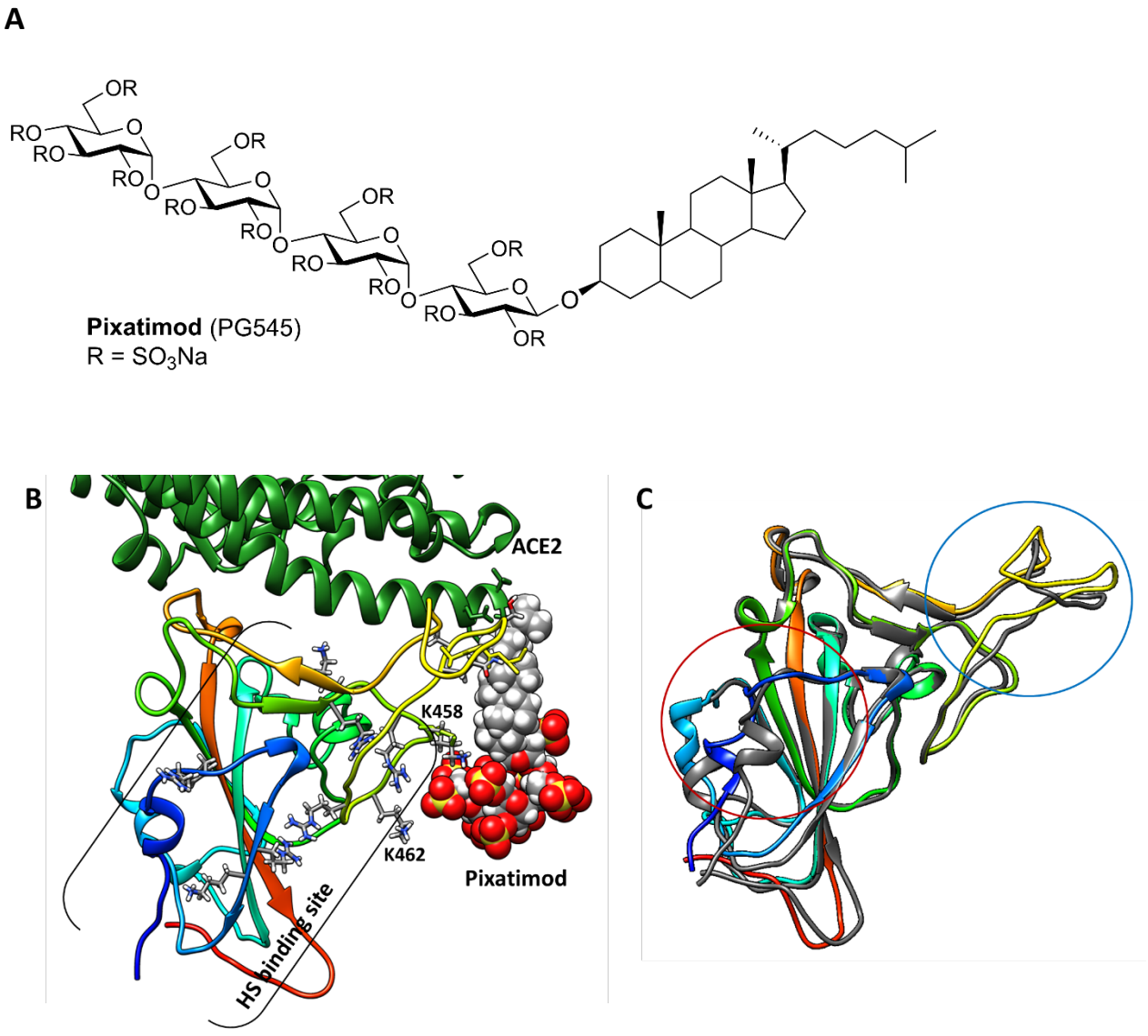

Figure 1: Molecular dynamics modelling defines direct interactions of pixatimod with S1 RBD: *A, Structure of pixatimod. B, Model showing interactions of pixatimod with the RBD domain of spike protein. The sulfated tetrasaccharide partially occupies the HS/heparin binding site. The lipophilic tail of*

pixatimod wraps around the hydrophobic loop, thereby creating a steric clash with the helix of ACE2 protein (shown in inset-green ribbon). C, Superimposition of the X-ray structure (PDB: 6LZG) and one of the snapshots from MD simulations (ligand not shown) suggest conformational change around the loop region (blue circle) and the N-terminal helix as highlighted (red circle).

Direct interaction of pixatimod with the spike protein S1 RBD

Spectroscopic studies with circular dichroism (CD) allow investigation of direct binding of compounds to recombinant spike protein receptor binding domain (S1 RBD). The RBD is the region of the protein spike which interacts with the ACE2 receptor on human cells. CD spectroscopy in the far UV region (λ = 190 - 260 nm) detects conformational changes in protein secondary structure that occur in solution and can infer binding by an added ligand. Such secondary structural changes can be quantified using spectral deconvolution. SARS-CoV-2 S1 RBD underwent conformational change in the presence of both pixatimod or heparin, consisting of decreased α-helical content for pixatimod and increased α-helix content for heparin (**Fig 2C**). A decrease in global β-sheet content is observed for both pixatimod and heparin, along with increases in turn structure (**Fig 2C**). The observed changes demonstrate that the SARS-CoV-2 S1 RBD interacts with pixatimod in aqueous conditions of physiological relevance. Notably, the conformational changes were distinct from those seen with heparin, suggesting different interactions with S1 RBD (**Fig 2**).

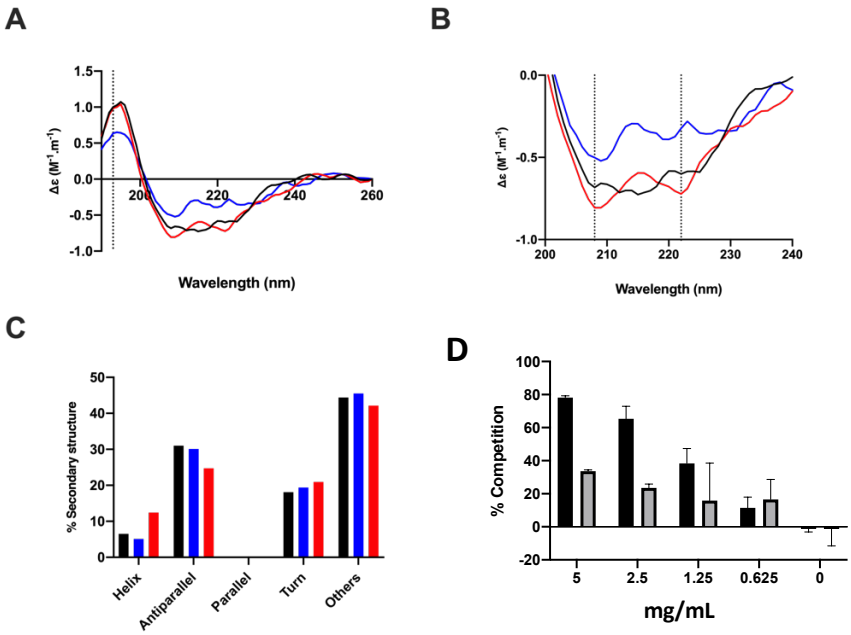

Figure 2: Pixatimod interacts with SARS-CoV-2 S1-RBD. *A, Circular dichroism spectra (190 - 260 nm) of SARS-CoV-2 S1RBD alone (black), or with heparin (red) or pixatimod (blue). The vertical dotted line indicates 193 nm. B, The same spectra expanded between 200 and 240 nm. Vertical dotted lines indicate 222 nm and 208 nm. C, Secondary structure content analysed using BeStSel for SARS-CoV-2 S1 RBD. α helical secondary structure is characterized by a positive band at ~193 nm and two negative bands at ~208 and ~222 nm (analysis using BeStSel was performed on smoothed data between 190 and 260 nm). D, Competitive ELISA of biotinylated heparin binding to immobilised S1 RBD. Heparin, solid bars, pixatimod, grey bars.*

To obtain further evidence that pixatimod interacts with S1 RBD, we performed competitive ELISA assays, assessing displacement of biotinylated heparin pre-bound to immobilized SARS-CoV-2 S1 RBD. Both heparin and pixatimod were able to displace heparin from S1 RBD (**Fig 2D**) though as we noted previously from surface plasmon resonance experiments on the interaction of S1 RBD to heparin (Mycroft-West, 2020c), relatively high concentrations (low mg/mL) are required for this displacement activity. Notably, pixatimod was less efficient than heparin at displacement, consistent with the modelling data indicating only partial overlap of their binding sites on S1 RBD (**Fig 1B**), and the additional avidity of heparin binding due to it containing multiple binding sites for S1 RBD.

Consistent with the modelling data, these data confirm direct interactions of pixatimod with S1 RBD, resulting in induction of a conformational change in S1 RBD. Taken together, these studies are consistent with the notion that HS mimetics such as pixatimod have the potential to block infectivity and cell-to-cell spread of SARS-CoV-2.

Pixatimod inhibits binding of S1 RBD binding to Vero cells

To assess the potential of pixatimod to inhibit SARS-CoV-2 binding to cells, we first evaluated inhibition of binding of His-tagged S1-RBD to monkey Vero cells. These cells are commonly used to measure binding and invasion by SARS-CoV-2, and are known to express both heparan sulfate proteoglycans (HSPGs) and the ACE2 protein receptor required for attachment and invasion of SARS-CoV-2. Fixed cells were exposed to His-tagged S1 RBD for 1hr, in the presence or absence of additional compounds, with subsequent washing and detection using a fluorescently-labelled anti-His tag antibody. A clear dose response was noted for both pixatimod and heparin (**Fig 3**), with 32% and 51% inhibition achieved at 100 µg/mL respectively. These data confirm that pixatimod can interfere with binding of S1 RBD to cells containing HSPGs and ACE2 protein receptor.

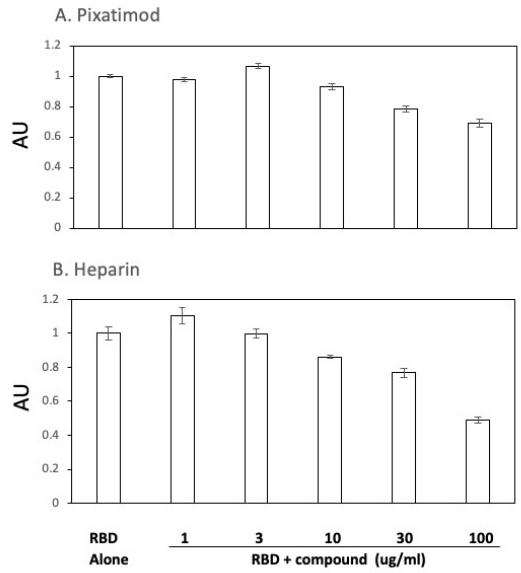

Figure 3: Pixatimod inhibits binding of S1-RBD to Vero cells. *The dose response effects of pixatimod (A) and unfractionated porcine mucosal heparin (B) on binding of S1-RBD to Vero cells. Data were normalised to control with no addition of S1 RBD. AU, arbitrary units of fluorescence.*

Antiviral effects of pixatimod in live virus assays

The effect of pixatimod on SARS-CoV-2 infection of Vero cells was examined using a standard plaque reduction assay. Pixatimod was pre-incubated with the SARS-CoV-2 Victoria isolate for 1 hr before infecting the cells. Significant decreases were observed in the number of PFU upon pixatimod treatment for SARS-CoV-2 **(Fig 4A**). Analysis of multiple dose response curves yielded an EC_{50} for pixatimod in the range of 2.4-13.8 μg/mL (mean 8.1 ug/ml; n=2 assays). In comparison, an EC_{50} of ~5-10 μg/ml has been observed for unfractionated heparin with a SARS-CoV-2 Italy UniSR1/2020 isolate (Mycroft-West, 2020c).

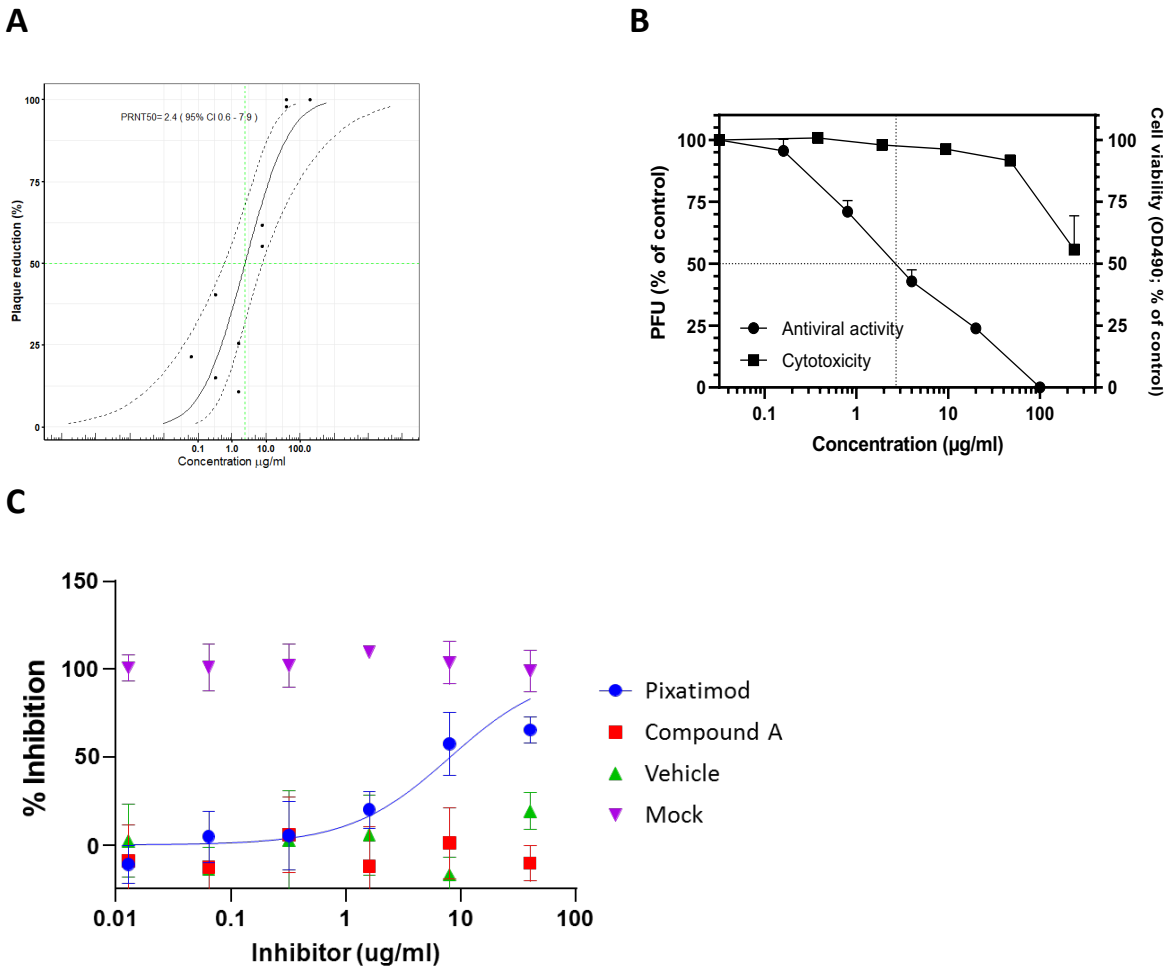

Figure 4: Pixatimod inhibits attachment and invasion of Vero cells by live SARS-CoV-2 virus isolates. *Live virus infectivity assays were performed as described in Methods for 3 different SARS-CoV-2 isolates. A, Plaque reduction assay of Victoria isolate, EC_{50} 2.4 ug/ml; B, Plaque reduction assay of DE isolate, EC_{50} 2.7 ug/ml; C, Cytopathic assay of QLD02 isolate, EC_{50} 8.0 ug/ml (representative examples shown). Results of pixatimod inhibition of SARS-CoV-2 infectivity are expressed as percent plaque reduction (A), plaque number as a percent of control (B), or percent inhibition from cytopathic effect (C). Panel B also shows cytotoxicity data for Vero cells for calculation of CC_{50} value (>236 ug/ml). In panel C, compound A is a control compound, octyl β-maltotetraoside tridecasulfate (Fig S3), an analogue of pixatimod which lacks the steroid side-chain.*

To establish that these antiviral effects were relevant for wider viral isolates, further complementary assays were conducted with a different SARS-CoV-2 viral isolate DE. To this end, pixatimod was also studied for its capability to inhibit infection of Vero cells by SARS-CoV-2 in a plaque reduction assay. Under these conditions, pixatimod inhibited infectivity of DE isolate with an EC_{50} value of 2.7 µg/mL (**Fig 4B**) which is similar to that found in some experiments with the Victoria isolate. Analysis of pixatimod cytotoxicity to Vero cells using a tetrazolium-based assay revealed that pixatimod decreased by 50% (CC_{50}) the viability of Vero cells at concentration >236 µg/mL, i.e., well above the EC_{50} values observed in the plaque reduction assay (**Fig. 4B; Table 1**). Selectivity index (SI) values for pixatimod ranged from >17 to >98 for these assays.

In addition to the plaque reduction assays, pixatimod inhibition of SARS-CoV-2 infectivity was assessed using assays that measured the cytopathic effects of the virus as an endpoint. Using the DE and the QLD02 isolates, EC50 for pixatimod inhibition of SARS-CoV-2 infectivity were determined to be 0.8-11.6 and 8.0 µg/mL, respectively (**Table 1**). These values were comparable with those observed for the plaque reduction assays (**Table 1**). We also noted that a "control" (Compound A, a pixatimod analogue lacking the steroid side-chain) (**Fig S3**) lacked efficacy (**Fig 4C**), demonstrating the importance of the steroid side-chain for activity of pixatimod.

The overall antiviral activity, cytotoxicity, and the selectivity index data for the three different isolates are summarised in Table 1, with SI values for pixatimod ranging from >17 to >295.

Table 1: Anti-SARS-CoV-2 activities of pixatimod in Vero cells

SARS-CoV-2 isolate	Assay Method	EC_{50} (µg/mL)	CC_{50} (µg/mL)	SI
Victoria isolate	Plaque reduction	8.1 (2.4-13.8)[a]	>236[c]	29 (>17 to >98[a])
DE isolate	Plaque reduction	2.7[a]		>87
	Cytopathic effect	0.8 – 11.6[b]		>20 to >295
QLD02 isolate	Cytopathic effect	8.0		>30

[a] Mean EC_{50} based on the data from two independent virus plaque reduction assays (individual assay $PRNT_{50}$, and resulting SI range, given in brackets).

[b] EC_{50} computed by the Reed and Muench formula based on the cytopathic effect assay. Range indicates upper (complete protection of cells) and lower (partial protection) limits of EC50 estimation.

[c] Cytotoxicity in Vero cells (determined at University of Gothenburg).

Discussion

The current COVID-19 pandemic illustrates the critical need to develop effective vaccines and therapeutics for viruses such as SARS-CoV-2. Established anti-viral agents appear to have limited utility against SARS-CoV-2. Owing to their use as a means of cell attachment by many viruses, HS represents an ideal broad-spectrum antiviral target (Cagno et al, 2019). Binding of a viral protein to cell-surface HS is often the first

step in a cascade of interactions that is required for viral entry and the initiation of infection (Lindahl and Li, 2020). As HS and heparin contain the same saccharide building blocks and HS-binding proteins also interact with heparin, this drug is gaining attention apart from its anticoagulant properties in COVID-19 treatment (Lindahl and Li, 2020). Heparin and HS have been recently shown to bind to S1 RBD (Mycroft-West, 2020a; Mycroft-West, 2020b; Liu, 2020), induce a conformational change in the S1 RBD of SARS-CoV-2 (Mycroft-West et al, 2020a) and inhibit cellular invasion by SARS-CoV-2 (Mycroft-West et al, 2020c). Heparin has also been shown to inhibit binding of SARS-SoV2 spike protein to a human cell line (Partridge, 2020), and to inhibit entry into human cells of pseudovirus carrying the SARS-CoV2 spike protein (Tandon, 2020). Moreover, low molecular weight heparins (LMWHs) may also have utility in COVID-19 as the SARS-CoV-2 spike S1 RBD undergoes conformational change upon interaction with some of these drugs (Mycroft-West et al., 2020b) and enoxaparin also inhibits pseudovirus entry (Tandon, 2020). Furthermore, in a retrospective clinical study LMWH treatment of COVID-19 patients was found to significantly lower plasma levels of IL-6, a key cytokine associated with the immunopathogenesis of the disease (Shi et al, 2020). However, the question of whether therapeutic doses of either UFH or LMWH should be considered for all COVID-19 patients as an anti-viral treatment is far from answered and it has been recommended that doses should be reserved for those who have confirmed thrombosis including filter thrombosis (Thacil et al, 2020). Indeed, case reports are beginning to emerge of serious bleeding complications in COVID-19 patients receiving LMWH which would suggest that the administration of heparin and LMWH as anti-viral agents is not without risk (Bargellini et al, 2020; Conti et al, 2020).

The potential of using HS oligosaccharides or related mimetics as therapeutic agents for COVID-19 is now gaining momentum based on recent data revealing that such compounds can inhibit SARS-CoV-2 binding to target cells. Furthermore, non-coagulating heparin or HS preparations can be developed that reduce cell binding and infectivity without a risk of causing bleeding (Liu et al., 2020). HS mimetics offer advantages in comparison to heparin such as avoiding interaction with antithrombin III which confers anticoagulant activity (Liu et al, 2020) and ready availability via synthetic chemistry production. Pixatimod (PG545) represents a clinical-stage HS mimetic with potential utility for the treatment and prevention of COVID-19.

To date, pixatimod has been administered as a once-weekly 1-hour intravenous infusion to over 80 cancer patients (unpublished) and is well tolerated, with predictable pharmacokinetics (PK) and no reports of heparin-induced thrombocytopenia (Dredge et al., 2018). The compound has mild anti-coagulant activity (Dredge et al, 2010) and is a single molecular entity prepared by total synthesis (Ferro et al, 2012). This is advantageous compared with unfractionated heparin (UFH) given heparin's issues with heterogeneity, less predictable PK, variable patient-dependent dose-responses, contamination risks and side effect profile, such as bleeding complications and heparin-induced thrombocytopenia (reviewed in Paluck et al, 2016). Though low molecular weight heparins (LMWHs) overcome some of these issues, they were optimized for anticoagulant rather than anti-viral activities, and their efficacy may be lower compared with heparin as they are less effective at binding to S1 RBD (Mycroft-West et al, 2020b) and inhibiting pseudovirus entry (Tandon, 2020). It is also noteworthy that heparin and LMWH are subject to the well known fragility of heparin's supply chain (Vilanova et al, 2019). Though pharmaceutical-grade UFH and LMWH preparations remain a polydisperse mixture of natural products, containing both anticoagulant and non-anticoagulant saccharide structures, these are considered an invaluable resource for development of next-generation antiviral agents that display negligible anticoagulant potential (Mycroft-West et al, 2020c).

As a clinical-stage HS mimetic, pixatimod provides better control over structure, molecular weight diversity (a single molecular entity), sulfation, purity and stability, all of which are attractive attributes for pharmaceutical products. Herein, we reveal a direct interaction of the clinical candidate pixatimod with the S1 spike protein RBD, supported by molecular modelling data. Pixatimod also inhibited the interaction of S1 RBD with Vero cells which are known to express the ACE2 receptor. Moreover, infectivity assays, of two types (plaque reduction and cytopathic effect, Table 1) confirm pixatimod is a potent inhibitor of SARS-CoV-2 infection of Vero cells with multiple different live SARS-CoV-2 virus isolates, at concentrations ranging from 0.8 to 13.8 μg/mL which are well within its known therapeutic range. The CC50 >100 μM (>236 μg/mL) in Vero cells is consistent with cytotoxicity data on human cells (CC50 or LC50). For example, >100 μM (>236 μg/mL) in human peripheral blood mononuclear cells (K. Dredge, personal communication), 78 μM (184 μg/mL) in endothelial cells, >100 μM (>236 μg/mL) in HepG2 cells or cancer cell lines (Dredge et al, 2011) and 63.5 μM (150 μg/mL) for Hec1B cells and 70.8 μM (167 μg/mL) for ARK2 cells (Hoffman et al, 2020) indicating that pixatimod is not cytotoxic *in vitro*. Importantly, the maximum plasma concentration (C_{max}) of pixatimod following a single treatment of 100 mg in cancer patients is 29.5 μg/mL with a C_{min} of 2.7 μg/mL measured one week following treatment (Dredge et al, 2018), indicating that the current dosing regimen should be sufficient to achieve antiviral activity in human subjects. The low anticoagulant activity of pixatimod is an advantage for its use as a direct antiviral agent, because it would provide the potential to develop optimized timing and dosing combination therapies with heparin or LMWHs, since they are being used to treat coagulopathies observed in COVID-19 patients (Tang, 2020).

It is notable that there are multiple potential mechanisms of action of pixatimod against SARS-CoV-2 and/or other viruses (highlighted in Fig 5). In addition to direct antiviral activity shown against SARS-CoV-2, pixatimod also has immunomodulatory effects which may alleviate some of the immunopathologies associated with moderate-severe COVID-19 patients. It inhibits the pro-inflammatory enzyme heparanase (Dredge et al, 2011) and has been demonstrated to suppress IL-6 in inflammatory (pancreatitis) and viral (Ross River virus) animal models in a process thought to be driven by elevated levels of heparanase (Khamaysi et al, 2017, Supramaniam et al, 2018). Moreover, it blocks the heparanase-dependent invasion of macrophages into tumours in mouse cancer models (Ostapoff et al, 2013; Boyango et al, 2014; Barash et al, 2018). In the context of viral infection, the invasion of monocytes and macrophages into the lungs is associated with severe COVID-19 disease (Merad and Martin, 2020), representing an immunopathology which may be heparanase-dependent and potentially responsive to agents such as pixatimod. Recent findings that the vaccinia virus relies on host heparanase to degrade HS in order to spread to distant sites (Khanna et al, 2019), sheds further light on another role of HS and heparanase in the progression of disease following viral infection that may also apply for COVID-19. Notably, increased plasma heparanase activity is also associated with COVID-19 (Buijsers et al, 2020).

Based on these data, pixatimod has potent antiviral activity against SARS-CoV-2 at therapeutically relevant concentrations in addition to its immunomodulatory properties which may support the host response to COVID-19 infection. This provides strong support to justify entry of pixatimod to clinical trials for COVID-19.

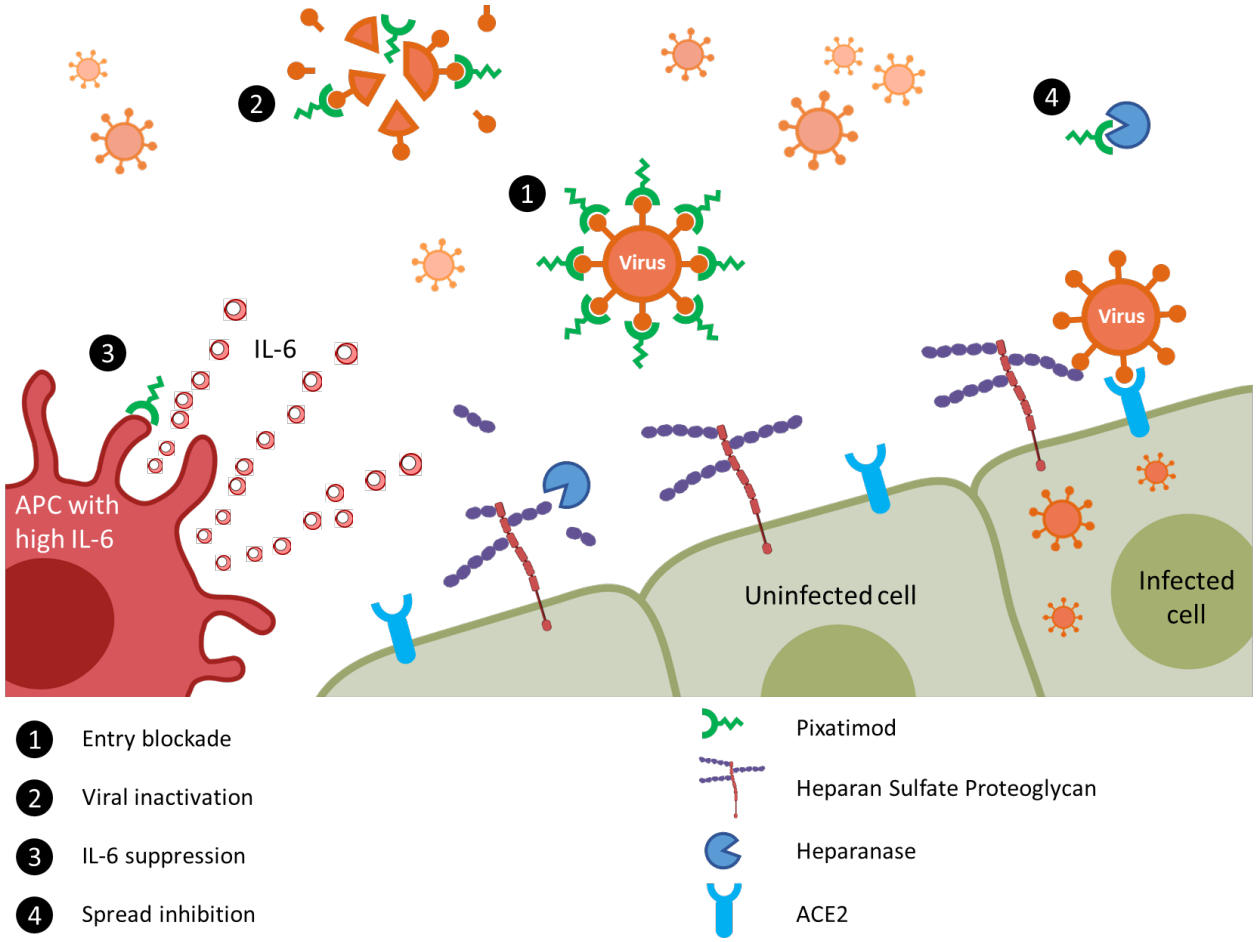

Figure 5: Proposed multi-mode mechanisms of pixatimod activity against SARS-CoV-2 and other viruses. *The principal mode of action demonstrated here is that pixatimod acts as a decoy receptor [1], blocking S1-RBD binding to HS co-receptors and inhibiting viral attachment to host cells, thus blocking viral infection. Additional potential modes of action include: [2] virucidal activity of pixatimod, dependent upon the cholestanol moiety (Said et al, 2016), which may lead to degradation and permanent inactivation of SARS-CoV-2 virus particles; [3] suppression of IL-6 secretion by antigen presenting cells, primarily macrophages (Khamaysi et al, 2017); and [4] blocking viral escape from host cell by inhibiting heparanase which otherwise promotes viral escape by cleaving HS receptors (Khanna et al, 2019; Buijsers et al, 2020).*

Experimental

Computational methods: The crystal structure of the RBD-ACE2 complex (PDB ID: 6LZG, Wang et al, 2020) was retrieved from the RCSB Protein Data Bank. Structures were stripped of water molecules, ACE2 chain and any cofactors and/or ligands present. UCSF Chimera was used to edit the structure and for visualisation. Without prior knowledge of the pixatimod binding site, one molecule of the ligand was placed in the simulation system containing the protein, solvent and ions and molecular dynamics (MD) simulations were performed for 600 ns. Such unguided simulations, as reviewed before (Ghanakota and

Carlson 2016; Shan et al, 2011), have been used to predict the binding sites on a protein's surface and drive the design of new ligands.

All the MD simulations were carried out using the pmemd.cuda module (Salomon-Ferrer et al, 2013) of the AMBER 16 molecular dynamics package and the analyses were performed using the cpptraj module of AmberTools16 (Case et al, 2005). Simulation systems were set up by placing the spike RBD domain at the centre of the octahedral simulation box (with an extension of at least 12 Å from each side). Pixatimod was randomly placed in the box. This was followed by addition of TIP3P water (Jorgensen et al, 1983) and Na^+ ions for neutralising the charge of the system. Proteins were parameterized using the Amber99SB-ildn force field (Lindorff-Larsen et al, 2010) whereas Glycam-06 (version j, Kirschner et al, 2008) and Lipid14 (Madej et al, 2015) force fields were used for the sulfated tetrasaccharide and cholestanol moieties of pixatimod, respectively. Four replicates of the unguided simulations were performed (4 × 600 ns). Periodic boundary conditions were applied, and the time step was set to 2 fs. The electrostatic energy was calculated with the particle mesh Ewald (PME) method. SHAKE constraints were applied on the bonds involving hydrogen. A cut-off of 12 Å was applied to the Lennard-Jones and direct space electrostatic interactions with a uniform density approximation included to correct for the long-range van der Waals interactions.

The system was first minimized without electrostatics for 500 steps, then with a restraint of 25 kcal/(mol $Å^2$) applied on the protein and pixatimod. This minimization was followed by 100-ps MD simulation with 25 kcal/(mol $Å^2$) positional restraints applied on the protein and ligand, and the temperature was slowly increased from 0 to 300 K. Then, followed by 500 steps of steepest descent cycles followed by 500 steps of conjugate gradient minimization, and 50-ps equilibrations with a restraint force constant of 5 kcal/(mol $Å^2$) in the protein and ligand, followed by final 2 ns equilibration without restraints to equilibrate the density. The first few steps were all carried out at constant volume followed by at least 600 ns production MD simulation at 300 K (Langevin dynamics, collision frequency: 5/ps) with 1-atm constant pressure. Trajectories were collected and data analyses such as RMSD, RMSF and free energy of binding were performed on the last 30000 frames. The binding free energy and pairwise residue contributions (Gohlke et al, 2003) were calculated using the Molecular mechanics-Generalized Born (GB) equation (MM/GBSA) procedure implemented in AmberTools16. The details of this method have been extensively reviewed (Genheden et al, 2015). The polar solvation energy contribution was calculated by using $GB^{OBC\ II}$ (igb= 5) (Onufriev et al, 2004). The value of the implicit solvent dielectric constant and the solute dielectric constant for GB calculations was set to 80 and 1, respectively. The solvent probe radius was set to 1.4 Å as default. The entropy calculation is computationally expensive and therefore not performed for the purposes of this study.

Expression of His-tagged recombinant SARS-CoV-2 S1 RBD: Residues 330−583 of the SARS-CoV-2 spike protein (GenBank: MN908947) were cloned upstream of a N-terminal 6XHisTag in the pRSETA expression vector and transformed into SHuffle® T7 Express Competent *E. coli* (NEB, UK). Protein expression was carried out in MagicMediaTM *E. coli* Expression Media (Invitrogen, UK) at 30°C for 24 hrs, 250 rpm. The bacterial pellet was suspended in 5 mL lysis buffer (BugBuster Protein Extraction Reagent, Merck Millipore, UK; containing DNAse) and incubated at room temperature for 30 mins. Protein was purified from inclusion bodies using IMAC chromatography under denaturing conditions. On-column protein refolding was performed by applying a gradient with decreasing concentrations of the denaturing agent (from 8M Urea). After extensive washing, protein was eluted using 20 mM NaH_2PO_4, pH 8.0, 300 mM NaCl, 500 mM imidazole. Fractions were pooled and buffer-exchanged to phosphate-buffered saline (PBS;

140 mM NaCl, 5 mM NaH_2PO_4, 5 mM Na_2HPO_4, pH 7.4; Lonza, UK) using Sephadex G-25 media (GE Healthcare, UK). Recombinant protein was stored at -4°C until required.

Secondary structure determination of SARS-CoV-2 S1 RBD by circular dichroism spectroscopy: The circular dichroism (CD) spectrum of the SARS-CoV-2 S1 RBD in PBS was recorded using a J-1500 Jasco CD spectrometer (Jasco, UK), Spectral Manager II software (JASCO, UK) and a 0.2 mm path length, quartz cuvette (Hellma, USA) scanning at 100 nm/min, with 1 nm resolution throughout the range λ = 190 - 260 nm. All spectra obtained were the mean of five independent scans, following instrument calibration with camphorsulfonic acid. SARS-CoV-2 S1 RBD was buffer-exchanged (prior to spectral analysis) using a 10 kDa Vivaspin centrifugal filter (Sartorius, Germany) at 12,000 g, thrice and CD spectra were collected using 21 µL of a 0.6 mg/mL solution in PBS, pH 7.4. Spectra of heparin (porcine mucosal heparin) were collected in the same buffer at approximately comparable concentrations, since this is a polydisperse material. Collected data were analysed with Spectral Manager II software prior to processing with GraphPad Prism 7, using second order polynomial smoothing through 21 neighbours. Secondary structural prediction was calculated using the BeStSel analysis server (Micsonai et al, 2015).

To ensure that the CD spectral change of SARS-CoV-2 S1 RBD in the presence of pixatimod did not arise from the addition of the compound alone, a difference spectrum was analysed. The theoretical CD spectrum that resulted from the arithmetic addition of the CD spectrum of the SARS-CoV-2 S1 RBD and that of pixatimod differed from the observed experimental CD spectrum of SARS-CoV-2 S1 RBD mixed with compound alone. This demonstrates that the change in the CD spectrum arose from a conformational change following binding to pixatimod [Supplementary Fig S4].

Displacement ELISA for S1 RBD binding to heparin: Greiner BioOne high binding 96 well plates were coated with 50 µL of 5 µg/mL SARS-CoV-2 RBD in 0.05 M sodium carbonate buffer pH 9.6 prior to incubation at 37°C for 1 hr. Plates were washed with PBS supplemented with 0.2% (w/v) Brij35 3 times before blocking with PBS supplemented with 2% (w/v) BSA and 0.2% (w/v) Brij35 for 1 hr at 37 °C. Plates were washed again 3 times with PBS supplemented with 0.2% (w/v) Brij35 and incubated with 50 µg/mL biotinylated heparin (Millipore) for 30 mins at 37 °C. After washing 3 times with PBS supplemented with 0.2% (w/v) Brij35 plates were incubated for 30 minutes with dilutions of unconjugated heparin (black) or pixatimod (grey). After further washing 3 times with 0.2% (w/v) Brij35, wells were incubated with 50 µL 0.1 µg/mL of an anti-biotin-HRP antibody (Invitrogen) for 30 minutes. Plates were washed extensively with PBS supplemented with 0.2% Brij 35 (5x) and detection was performed using 50 µL of TMB solution (Sigma-Aldrich). Colour development was stopped using 2M H_2SO_4 after 10 minutes and the absorbance at 450 nm ascertained. % Competition values were calculated between controls with no test compound (0%) and no SARS-CoV-2 RBD protein controls (representing background; 100%).

Cell binding of S1 RBD: African green monkey Vero kidney epithelial cells (Vero E6) were purchased from ATCC. Cells were maintained at 50-75% confluence in DMEM supplemented with 10% foetal bovine serum, 20 mM L-glutamine, 100 U/mL penicillin-G and 100 U/mL streptomycin sulfate (all purchased from Gibco/ThermoFisher, UK). Cells were maintained at 37 °C, in 5% CO_2 and plated into 96-well cell culture plates at 1000 cells/well in 100 µL of maintenance medium. Cells were allowed to adhere overnight. Medium was aspirated and wells were washed 3x with 200 µL calcium, magnesium-free PBS (CMF-PBS, Lonza, UK). Cells were fixed with 100 µL 10% neutral buffered Formalin (Thermofisher, UK) for 10 minutes at room temperature, then washed 3x with 200 µL CMF-PBS. 100 µL CMF-PBS was added to each well and plates were stored at 4 °C until use. Before use, wells were blocked with 200 µL CMF-PBS + 1% BSA

(Sigma-Roche, UK) for 1 hour at room temperature, and washed 3x with 200 µL CMF-PBS + 0.1% Tween-20 (PBST, Sigma-Roche, UK) followed by 2x with 200 µL CMF-PBS.

His-tagged S1-RBD (50 µg/mL) and compounds at indicated concentrations were added to each well in 25 µL PBST + 0.1% BSA as indicated. Wells were incubated for 1 hour at room temperature with rocking. Wells were washed 3x with 200 µL PBST and 2x with 200 µL CMF-PBS. Binding of His-tagged S1-RBD was detected with Alexa Fluor 488 anti-his tag antibody (clone J095G46, Biolegend, UK) 1:5000 in 25 µL PBST + 0.1% BSA per well. Wells were incubated in the dark for 1 hour at room temperature with rocking. Wells were washed 3x with 200 µL PBST and 2x with 200 µL CMF-PBS. Fluorescence was read at Ex. 485:Em 535 on a Tecan Infinite M200Pro plate reader. Results are presented as normalized mean (where 0 is the fluorescence without added S1-RBD, and 1 is the fluorescence with 50 µg/mL S1-RBD; ±%CV, n=3).

Live SARS-CoV-2 virus assays:

SARS-CoV-2 Victoria isolate: a plaque reduction assay was performed with the SARS-CoV-2 Victoria/01/2020 (passage 3) isolate, diluted to a concentration of 1.4 x 10^3 pfu/mL (70 pfu/50µL) in minimal essential media (MEM) (Life Technologies, California, USA) containing 1% (v/v) foetal calf serum (FCS) (Life Technologies) and 25 mM HEPES buffer (Sigma) and mixed 50:50 with pixatimod dilutions, in a 96-well V-bottomed plate. The plate was incubated at 37 °C in a humidified box for 1 hour to allow the virus to be exposed to pixatimod. The virus-compound mixture was transferred onto the wells of a washed 24-well plate that had been seeded with Vero E6 cells [ECACC 85020206] the previous day at 1.5 x 10^5 cells/well. The virus-compound mixture was left to adsorb for an hour at 37°C, then plaque assay overlay media was applied (MEM containing 1.5% carboxymethylcellulose (Sigma, Dorset, UK), 4% (v/v) FCS and 25 mM HEPES buffer). After incubation at 37 °C in a humidified box, for 5 days, plates were fixed overnight with 20% (v/v) formalin/PBS, washed with tap water and then stained with methyl crystal violet solution (0.2% v/v) (Sigma) and plaques were counted. Compound dilutions were performed in either duplicate or quadruplicate. Compound dilutions and cells only were run in duplicate, to determine if there was any cell cytotoxicity. A mid-point probit analysis (written in R programming language for statistical computing and graphics) was used to determine the amount (µg/mL) required to reduce SARS-CoV-2 viral plaques by 50% (PRNT50) compared with the virus only control (n=5). An internal positive control for the PRNT assay was run in triplicate using a sample of heat-inactivated human MERS convalescent serum known to neutralise SARS-CoV-2 (National Institute for Biological Standards and Control, UK).

SARS-CoV-2 DE isolate: Plaque reduction assay for SARS-CoV-2 isolate DE was performed in a similar manner, except for the virus and the pixatimod (fivefold decreasing concentrations at a range 100-0.16 µg/ml) were diluted in DMEM supplemented with 2% heat-inactivated FCS, and 100 U of penicillin and 60 µg/ml of streptomycin (DMEM-S). The virus (100 PFU) and pixatimod (fivefold decreasing concentrations at a range 100 – 0.16 µg/ml) were mixed and incubated for 30 min in humidified atmosphere comprising 5% CO_2 (CO_2 incubator). The mixtures were then transferred to Vero E6 cells and following incubation with cells for 90 min in the CO_2 incubator, the methylcellulose overlay was added. Three separate experiments each with duplicates were performed.

A cytopathic effect assay was performed with the SARS-CoV-2 DE isolate and Vero E6 cells (ECACC) plated at 2 x 10^4 per well in 96-well plates the day prior to the experiment. Serial fivefold dilutions of pixatimod in DMEM supplemented with 2% heat-inactivated FCS, and 100 U of penicillin and 60 µg/mL of streptomycin(DMEM-S) were incubated with 100 TCID50 of SARS-CoV-2 isolate DE for 20 min in

humidified atmosphere comprising 5% CO_2 (CO_2 incubator). The final concentrations of pixatimod were in a range 0.075 µg/mL to 47.2 µg/mL. The cells were rinsed once with 50 µL of DMEM-S, and then 200 µL of the virus-pixatimod mixtures were added to each well with cells (in quadruplicates). After incubation of the virus-pixatimod mixtures with cells for 3 days in the CO_2 incubator, the cells were inspected under a microscope for the presence of virus induced cytopathic effect where complete protection of cells were denoted as "+" while a partial protection (~50% of cells showing no cytopathic effect) was recorded as "+/-". The 50% end-point (EC50) was computed by the Reed and Muench method (Reed and Muench, 1938).

SARS-CoV-2 QLD02 isolate: A cytopathic effect assay was carried out as described above for the DE isolate, with 10 ffu/well and 3 days incubation. In this assay, Vero E6 cells were plated at 2 x 10^4 per well in 96-well plates the day prior to experiment. Serial five-fold dilutions of pixatimod in DMEM supplemented with 2% heat-inactivated FCS, and 100 U of penicillin and 60 µg/mL of streptomycin (DMEM-S) were incubated with 10 foci forming units of SARS-CoV-2 isolate QLD02 and incubated for 30 min in humidified atmosphere comprising 5% CO_2 (CO_2 incubator). The cells were rinsed once with 50 µL of DMEM-S, and then 200 µL of the virus-pixatimod mixtures were added to each well with cells (in triplicates). After incubation of the virus-pixatimod mixtures with cells for 3 days in the CO_2 incubator, the cells were fixed with 4% PFA and then stained with crystal violet. Then crystal violet was released by methanol and OD495 was measured to quantify cell viability (protection from infection). The EC50 was then calculated using Prism.

Cytotoxicity assays: The assay was performed as described by Lundin *et al*. (2012). Briefly, Vero cells (2 x 10^4 cells/well) were seeded in 96 well cluster plates to become nearly confluent at the day of the experiment. The cell growth medium was then removed and 100 µL of serial fivefold dilutions of pixatimod in DMEM-S (ranging from 0.09 to 236 µg/mL) were added to cells. Following incubation of cells with pixatimod for 3 days in the CO_2 incubator, 20 µL of the MTS salt containing CellTiter 96 Aqueous One Solution reagent (Promega, Madison, WI) was added and incubated for further 1-2 h at 37 °C. The absorbance was recorded at 490 nm against a background of 650 nm. Two separate experiments each in duplicates were performed and the results are expressed as percentage of absorbance value detected with pixatimod relative to control cells.

Acknowledgements

The authors would like to thank Zucero Therapeutics for provision of pixatimod (PG545) and Queensland Health Forensic & Scientific Services, Queensland Department of Health for provision of QLD02 SARS-CoV-2 isolate. V.F. acknowledges support from the Australian Research Council (DP170104431). TB acknowledges support of the Swedish Research Council. AAK acknowledges funding support from the Australian Infectious Diseases Research Centre. Computational (and/or data visualisation) resources and services used in this work were provided by the eResearch Office, Queensland University of Technology, Brisbane, Australia and with the assistance of resources from the National Computational Infrastructure (NCI Australia), an NCRIS enabled capability supported by the Australian Government. N.S.G. is supported through the Advance Queensland Industry Research Fellowship.

Conflict of Interest

E.H. and K.D. are employees of Zucero Therapeutics. V.F., E.H. and K.D. are inventors on pixatimod patents.

References

Abassi, Z., Hamoud, S., Hassan, A., Khamaysi, I., Nativ, O., Heyman, S.N., Muhammad, R.S., Ilan, N., Singh, P., Hammond, E., Zaza, G., Lupo, A., Onisto, M., Bellin, G., Masola, V., Vlodavsky, I., and Gambaro, G. (2017). Involvement of heparanase in the pathogenesis of acute kidney injury: nephroprotective effect of PG545. *Oncotarget* 8**,** 34191-34204.

Ackermann, M., Verleden, S.E., Kuehnel, M., Haverich, A., Welte, T., Laenger, F., Vanstapel, A., Werlein, C., Stark, H., Tzankov, A., Li, W.W., Li, V.W., Mentzer, S.J., and Jonigk, D. (2020). Pulmonary Vascular Endothelialitis, Thrombosis, and Angiogenesis in Covid-19. *N Engl J Med*.

Akhmerov, A., and Marbán, E. (2020). COVID-19 and the Heart. *Circ Res* 126**,** 1443-1455.

Barash, U., Lapidot, M., Zohar, Y., Loomis, C., Moreira, A., Feld, S., Goparaju, C., Yang, H., Hammond, E., Zhang, G., Li, J.P., Ilan, N., Nagler, A., Pass, H.I., and Vlodavsky, I. (2018). Involvement of Heparanase in the Pathogenesis of Mesothelioma: Basic Aspects and Clinical Applications. *J Natl Cancer Inst* 110**,** 1102-1114.

Bargellini, I., Cervelli, R., Lunardi, A., Scandiffio, R., Daviddi, F., Giorgi, L., Cicorelli, A., Crocetti, L., and Cioni, R. (2020). Spontaneous Bleedings in COVID-19 Patients: An Emerging Complication. *Cardiovasc Intervent Radiol***,** 1-2.

Boyango, I., Barash, U., Naroditsky, I., Li, J.P., Hammond, E., Ilan, N., and Vlodavsky, I. (2014). Heparanase cooperates with Ras to drive breast and skin tumorigenesis. *Cancer Res* 74**,** 4504-4514.

Buijsers, B., Yanginlar, C., de Nooijer, A., Grondman, I., Maciej-Hulme, M.L., Jonkman, I., Janssen, N.A.F., Rother, N., de Graaf, M., Pickkers, P., Kox, M., Joosten, L.A.B., Nijenhuis, T., Netea, M.G., Hilbrands, L., van de Veerdonk, F.L., Duivenvoorden, R., de Mast, Q & van der Vlag J. (2020) Increased plasma heparanase activity in COVID-19 patients *medRxiv* 2020.06.12.20129304.

Cagno, V., Tseligka, E.D., Jones, S.T., and Tapparel, C. (2019). Heparan Sulfate Proteoglycans and Viral Attachment: True Receptors or Adaptation Bias? *Viruses* 11.

Case, D.A., Cheatham Iii, T.E., Darden, T., Gohlke, H., Luo, R., Merz Jr, K.M., Onufriev, A., Simmerling, C., Wang, B., and Woods, R.J. (2005). The Amber biomolecular simulation programs. *Journal of computational chemistry* 26**,** 1668-1688.

Chan, L., Chaudhary, K., Saha, A., Chauhan, K., Vaid, A., Baweja, M., Campbell, K., Chun, N., Chung, M., Deshpande, P., Farouk, S.S., Kaufman, L., Kim, T., Koncicki, H., Lapsia, V., Leisman, S., Lu, E., Meliambro, K., Menon, M.C., Rein, J.L., Sharma, S., Tokita, J., Uribarri, J., Vassalotti, J.A., Winston, J., Mathews, K.S., Zhao, S., Paranjpe, I., Somani, S., Richter, F., Do, R., Miotto, R., Lala, A., Kia, A., Timsina, P., Li, L., Danieletto, M., Golden, E., Glowe, P., Zweig, M., Singh, M., Freeman, R., Chen, R., Nestler, E., Narula, J., Just, A.C., Horowitz, C., Aberg, J., Loos, R.J.F., Cho, J., Fayad, Z., Cordon-Cardo, C., Schadt, E., Levin, M.A., Reich, D.L., Fuster, V., Murphy, B., He, J.C., Charney, A.W., Bottinger, E.P., Glicksberg, B.S., Coca, S.G., and Nadkarni, G.N. (2020). Acute Kidney Injury in Hospitalized Patients with COVID-19. *medRxiv*.

Conti, C.B., Henchi, S., Coppeta, G.P., Testa, S., and Grassia, R. (2020). Bleeding in COVID-19 severe pneumonia: The other side of abnormal coagulation pattern? *Eur J Intern Med*.

Dredge, K., Brennan, T.V., Hammond, E., Lickliter, J.D., Lin, L., Bampton, D., Handley, P., Lankesheer, F., Morrish, G., Yang, Y., Brown, M.P., and Millward, M. (2018). A Phase I study of the novel immunomodulatory agent PG545 (pixatimod) in subjects with advanced solid tumours. *Br J Cancer* 118**,** 1035-1041.

Dredge, K., Hammond, E., Davis, K., Li, C.P., Liu, L., Johnstone, K., Handley, P., Wimmer, N., Gonda, T.J., Gautam, A., Ferro, V., and Bytheway, I. (2010). The PG500 series: novel heparan sulfate mimetics as potent angiogenesis and heparanase inhibitors for cancer therapy. *Invest New Drugs* 28**,** 276-283.

Dredge, K., Hammond, E., Handley, P., Gonda, T.J., Smith, M.T., Vincent, C., Brandt, R., Ferro, V., and Bytheway, I. (2011). PG545, a dual heparanase and angiogenesis inhibitor, induces potent anti-tumour and anti-metastatic efficacy in preclinical models. *Br J Cancer* 104**,** 635-642.

Ekblad, M., Adamiak, B., Bergstrom, T., Johnstone, K.D., Karoli, T., Liu, L., Ferro, V., and Trybala, E. (2010). A highly lipophilic sulfated tetrasaccharide glycoside related to muparfostat (PI-88) exhibits virucidal activity against herpes simplex virus. *Antiviral Res* 86**,** 196-203.

Ferro, V., Liu, L., Johnstone, K.D., Wimmer, N., Karoli, T., Handley, P., Rowley, J., Dredge, K., Li, C.P., Hammond, E., Davis, K., Sarimaa, L., Harenberg, J., and Bytheway, I. (2012). Discovery of PG545: a highly potent and simultaneous inhibitor of angiogenesis, tumor growth, and metastasis. *J Med Chem* 55**,** 3804-3813.

Genheden, S., and Ryde, U. (2015). The MM/PBSA and MM/GBSA methods to estimate ligand-binding affinities. *Expert Opin Drug Discov* 10**,** 449-461.

Ghanakota, P., and Carlson, H.A. (2016). Moving Beyond Active-Site Detection: MixMD Applied to Allosteric Systems. *J Phys Chem B* 120**,** 8685-8695.

Gohlke, H., Kiel, C., and Case, D.A. (2003). Insights into protein-protein binding by binding free energy calculation and free energy decomposition for the Ras-Raf and Ras-RalGDS complexes. *J Mol Biol* 330**,** 891-913.

Guan, W.-J., Ni, Z.-Y., Hu, Y., Liang, W.-H., Ou, C.-Q., He, J.-X., Liu, L., Shan, H., Lei, C.-L., Hui, D.S.C., Du, B., Li, L.-J., Zeng, G., Yuen, K.-Y., Chen, R.-C., Tang, C.-L., Wang, T., Chen, P.-Y., Xiang, J., Li, S.-Y., Wang, J.-L., Liang, Z.-J., Peng, Y.-X., Wei, L., Liu, Y., Hu, Y.-H., Peng, P., Wang, J.-M., Liu, J.-Y., Chen, Z., Li, G., Zheng, Z.-J., Qiu, S.-Q., Luo, J., Ye, C.-J., Zhu, S.-Y., and Zhong, N.-S. (2020). Clinical Characteristics of Coronavirus Disease 2019 in China. *New England Journal of Medicine* 382**,** 1708-1720.

Hammond, E., Haynes, N.M., Cullinane, C., Brennan, T.V., Bampton, D., Handley, P., Karoli, T., Lanksheer, F., Lin, L., Yang, Y., and Dredge, K. (2018). Immunomodulatory activities of pixatimod: emerging nonclinical and clinical data, and its potential utility in combination with PD-1 inhibitors. *J Immunother Cancer* 6**,** 54.

Hoffmann, M., Kleine-Weber, H., Schroeder, S., Krüger, N., Herrler, T., Erichsen, S., Schiergens, T.S., Herrler, G., Wu, N.H., Nitsche, A., Müller, M.A., Drosten, C., and Pöhlmann, S. (2020). SARS-CoV-2 Cell Entry Depends on ACE2 and TMPRSS2 and Is Blocked by a Clinically Proven Protease Inhibitor. *Cell* 181**,** 271-280.e278.

Jorgensen, W.L., Chandrasekhar, J., Madura, J.D., Impey, R.W., and Klein, M.L. (1983). Comparison of simple potential functions for simulating liquid water. *The Journal of Chemical Physics* 79**,** 926-935.

Khamaysi, I., Singh, P., Nasser, S., Awad, H., Chowers, Y., Sabo, E., Hammond, E., Gralnek, I., Minkov, I., Noseda, A., Ilan, N., Vlodavsky, I., and Abassi, Z. (2017). The Role of Heparanase in the Pathogenesis of Acute Pancreatitis: A Potential Therapeutic Target. *Sci Rep* 7**,** 715.

Khanna, M., Ranasinghe, C., Browne, A.M., Li, J.P., Vlodavsky, I., and Parish, C.R. (2019). Is host heparanase required for the rapid spread of heparan sulfate binding viruses? *Virology* 529**,** 1-6.

Kirschner, K.N., Yongye, A.B., Tschampel, S.M., González-Outeiriño, J., Daniels, C.R., Foley, B.L., and Woods, R.J. (2008). GLYCAM06: a generalizable biomolecular force field. Carbohydrates. *J Comput Chem* 29**,** 622-655.

Koliesnik, I.O., Kuipers, H.F., Medina, C.O., Zihsler, S., Liu, D., Van Belleghem, J.D., and Bollyky, P.L. (2020). The Heparan Sulfate Mimetic PG545 Modulates T Cell Responses and Prevents Delayed-Type Hypersensitivity. *Front Immunol* 11**,** 132.

Kuo, J., Bampton, D., Lemech, C., Brown, M., Stanley, A., Chojnowski, G., Hammond, E., Dredge, K., and Goldstein, D. (Year). "Preliminary results from a Phase Ib study of pixatimod (PG545) in combination with nivolumab in patients with advanced solid tumours with an expansion cohort in patients with metastatic pancreatic cancer", in: *EUROPEAN JOURNAL OF CANCER*: ELSEVIER SCI LTD THE BOULEVARD, LANGFORD LANE, KIDLINGTON, OXFORD OX5 1GB …), E18-E19.

Lamers, M.M., Beumer, J., Van Der Vaart, J., Knoops, K., Puschhof, J., Breugem, T.I., Ravelli, R.B.G., Paul Van Schayck, J., Mykytyn, A.Z., Duimel, H.Q., Van Donselaar, E., Riesebosch, S., Kuijpers, H.J.H., Schippers, D., Van De Wetering, W.J., De Graaf, M., Koopmans, M., Cuppen, E., Peters, P.J., Haagmans, B.L., and Clevers, H. (2020). SARS-CoV-2 productively infects human gut enterocytes. *Science*.

Lan, J., Ge, J., Yu, J., Shan, S., Zhou, H., Fan, S., Zhang, Q., Shi, X., Wang, Q., Zhang, L., and Wang, X. (2020). Structure of the SARS-CoV-2 spike receptor-binding domain bound to the ACE2 receptor. *Nature* 581**,** 215-220.

Lang, J., Yang, N., Deng, J., Liu, K., Yang, P., Zhang, G., and Jiang, C. (2011). Inhibition of SARS pseudovirus cell entry by lactoferrin binding to heparan sulfate proteoglycans. *PLoS One* 6**,** e23710.

Li, J.P., and Kusche-Gullberg, M. (2016). Heparan Sulfate: Biosynthesis, Structure, and Function. *Int Rev Cell Mol Biol* 325**,** 215-273.

Lindahl, U., and Li, J.P. (2020). Heparin - an old drug with multiple potential targets in Covid-19 therapy. *J Thromb Haemost*.

Lindorff-Larsen, K., Piana, S., Palmo, K., Maragakis, P., Klepeis, J.L., Dror, R.O., and Shaw, D.E. (2010). Improved side-chain torsion potentials for the Amber ff99SB protein force field. *Proteins* 78**,** 1950-1958.

Liu, J., and Thorp, S.C. (2002). Cell surface heparan sulfate and its roles in assisting viral infections. *Med Res Rev* 22**,** 1-25.

Liu, L., Chopra, P., Li, X., Wolfert, M.A., Tompkins, S.M., and Boons, G.J. (2020). SARS-CoV-2 spike protein binds heparan sulfate in a length- and sequence-dependent manner. *bioRxiv*.

Lundin, A., Bergström, T., Andrighetti-Fröhner, C.R., Bendrioua, L., Ferro, V., and Trybala, E. (2012). Potent anti-respiratory syncytial virus activity of a cholestanol-sulfated tetrasaccharide conjugate. *Antiviral Res* 93**,** 101-109.

Madej, B.D., Gould, I.R., and Walker, R.C. (2015). A Parameterization of Cholesterol for Mixed Lipid Bilayer Simulation within the Amber Lipid14 Force Field. *J Phys Chem B* 119**,** 12424-12435.

Martinez, M.A. (2020). Compounds with Therapeutic Potential against Novel Respiratory 2019 Coronavirus. *Antimicrob Agents Chemother* 64.

Merad, M., and Martin, J.C. (2020). Pathological inflammation in patients with COVID-19: a key role for monocytes and macrophages. *Nat Rev Immunol* 20**,** 355-362.

Micsonai, A., Wien, F., Kernya, L., Lee, Y.H., Goto, Y., Réfrégiers, M., and Kardos, J. (2015). Accurate secondary structure prediction and fold recognition for circular dichroism spectroscopy. *Proc Natl Acad Sci U S A* 112**,** E3095-3103.

Milewska, A., Zarebski, M., Nowak, P., Stozek, K., Potempa, J., and Pyrc, K. (2014). Human coronavirus NL63 utilizes heparan sulfate proteoglycans for attachment to target cells. *J Virol* 88**,** 13221-13230.

Modhiran, N., Gandhi, N.S., Wimmer, N., Cheung, S., Stacey, K., Young, P.R., Ferro, V., and Watterson, D. (2019). Dual targeting of dengue virus virions and NS1 protein with the heparan sulfate mimic PG545. *Antiviral Res* 168**,** 121-127.

Mycroft-West, C., Su, D., Elli, S., Guimond, S., Miller, G., Turnbull, J., Yates, E., Guerrini, M., Fernig, D., Lima, M., and Skidmore, M. (2020a). The 2019 coronavirus (SARS-CoV-2) surface protein (Spike) S1 Receptor Binding Domain undergoes conformational change upon heparin binding. *bioRxiv***,** 2020.2002.2029.971093.

Mycroft-West, C.J., Su, D., Li, Y., Guimond, S.E., Rudd, T.R., Elli, S., Miller, G., Nunes, Q.M., Procter, P., Bisio, A., Forsyth, N.R., Turnbull, J.E., Guerrini, M., Fernig, D.G., Yates, E.A., Lima, M.A., and Skidmore, M.A. (2020b). SARS-CoV-2 Spike S1 Receptor Binding Domain undergoes Conformational Change upon Interaction with Low Molecular Weight Heparins. *bioRxiv***,** 2020.2004.2029.068486.

Mycroft-West, C.J., Su, D., Pagani, I., Rudd, T.R., Elli, S., Guimond, S.E., Miller, G., Meneghetti, M.C.Z., Nader, H.B., Li, Y., Nunes, Q.M., Procter, P., Mancini, N., Clementi, M., Forsyth, N.R., Turnbull, J.E., Guerrini, M., Fernig, D.G., Vicenzi, E., Yates, E.A., Lima, M.A., and Skidmore, M.A. (2020c). Heparin inhibits cellular invasion by SARS-CoV-2: structural dependence of the interaction of the surface protein (spike) S1 receptor binding domain with heparin. *bioRxiv***,** 2020.2004.2028.066761.

Onufriev, A., Bashford, D., and Case, D.A. (2004). Exploring protein native states and large-scale conformational changes with a modified generalized born model. *Proteins* 55**,** 383-394.

Ostapoff, K.T., Awasthi, N., Cenik, B.K., Hinz, S., Dredge, K., Schwarz, R.E., and Brekken, R.A. (2013). PG545, an angiogenesis and heparanase inhibitor, reduces primary tumor growth and metastasis in experimental pancreatic cancer. *Mol Cancer Ther* 12**,** 1190-1201.

Paluck, S.J., Nguyen, T.H., and Maynard, H.D. (2016). Heparin-Mimicking Polymers: Synthesis and Biological Applications. *Biomacromolecules* 17**,** 3417-3440.

Partridge, L.J., Green, L.R., Monk, P.N. (2020) Unfractionated heparin potently inhibits the binding of SARS-CoV-2 spike protein to a human cell line. *bioRxiv***,** 2020.05.21.107870

Reed, L.J., and Muench, H. (1938). A simple method of estimating fifty per cent endpoints. *American journal of epidemiology* 27**,** 493-497.

Renu, K., Prasanna, P.L., and Valsala Gopalakrishnan, A. (2020). Coronaviruses pathogenesis, comorbidities and multi-organ damage - A review. *Life Sci* 255**,** 117839.

Said, J., Trybala, E., Andersson, E., Johnstone, K., Liu, L., Wimmer, N., Ferro, V., and Bergström, T. (2010). Lipophile-conjugated sulfated oligosaccharides as novel microbicides against HIV-1. *Antiviral Res* 86**,** 286-295.

Said, J.S., Trybala, E., Görander, S., Ekblad, M., Liljeqvist, J., Jennische, E., Lange, S., and Bergström, T. (2016). The Cholestanol-Conjugated Sulfated Oligosaccharide PG545 Disrupts the Lipid Envelope of Herpes Simplex Virus Particles. *Antimicrob Agents Chemother* 60**,** 1049-1057.

Salomon-Ferrer, R., Götz, A.W., Poole, D., Le Grand, S., and Walker, R.C. (2013). Routine Microsecond Molecular Dynamics Simulations with AMBER on GPUs. 2. Explicit Solvent Particle Mesh Ewald. *Journal of Chemical Theory and Computation* 9**,** 3878-3888.

Shan, Y., Kim, E.T., Eastwood, M.P., Dror, R.O., Seeliger, M.A., and Shaw, D.E. (2011). How does a drug molecule find its target binding site? *J Am Chem Soc* 133**,** 9181-9183.

Shang, J., Ye, G., Shi, K., Wan, Y., Luo, C., Aihara, H., Geng, Q., Auerbach, A., and Li, F. (2020). Structural basis of receptor recognition by SARS-CoV-2. *Nature* 581**,** 221-224.

Shi, C., Wang, C., Wang, H., Yang, C., Cai, F., Zeng, F., Cheng, F., Liu, Y., Zhou, T., and Deng, B. (2020). The potential of low molecular weight heparin to mitigate cytokine storm in severe COVID-19 patients: a retrospective clinical study. *Medrxiv*.

Supramaniam, A., Liu, X., Ferro, V., and Herrero, L.J. (2018). Prophylactic Antiheparanase Activity by PG545 Is Antiviral In Vitro and Protects against Ross River Virus Disease in Mice. *Antimicrob Agents Chemother* 62.

Tandon, R., Sharp, J.S., Zhang, F., Pomin, V.H., Ashpole, N.M., Mitra, D., Jin, W., Liu, H., Sharma, P., and Linhardt, R.J. (2020) Effective Inhibition of SARS-CoV-2 Entry by Heparin and Enoxaparin Derivatives. *bioRxiv*, 2020.06.08.140236

Tang, N., Bai, H., Chen, X., Gong, J., Li, D., Sun, Z. (2020) Anticoagulant treatment is associated with decreased mortality in severe coronavirus disease 2019 patients with coagulopathy. *J Thrombosis Haemostasis*. 18:1094–1099

Thachil, J., Tang, N., Gando, S., Falanga, A., Levi, M., Clark, C., Iba, T., and Cattaneo, M. (2020). Type and dose of heparin in Covid-19: Reply. *J Thromb Haemost*.

Varga, Z., Flammer, A.J., Steiger, P., Haberecker, M., Andermatt, R., Zinkernagel, A.S., Mehra, M.R., Schuepbach, R.A., Ruschitzka, F., and Moch, H. (2020). Endothelial cell infection and endotheliitis in COVID-19. *Lancet* 395, 1417-1418.

Vicenzi, E., Canducci, F., Pinna, D., Mancini, N., Carletti, S., Lazzarin, A., Bordignon, C., Poli, G., and Clementi, M. (2004). Coronaviridae and SARS-associated coronavirus strain HSR1. *Emerg Infect Dis* 10, 413-418.

Vilanova, E., Tovar, A.M.F., and Mourão, P.a.S. (2019). Imminent risk of a global shortage of heparin caused by the African Swine Fever afflicting the Chinese pig herd. *J Thromb Haemost* 17, 254-256.

Wang, Q., Zhang, Y., Wu, L., Niu, S., Song, C., Zhang, Z., Lu, G., Qiao, C., Hu, Y., Yuen, K.Y., Wang, Q., Zhou, H., Yan, J., and Qi, J. (2020). Structural and Functional Basis of SARS-CoV-2 Entry by Using Human ACE2. *Cell* 181, 894-904.e899.

Who (2020). "Coronavirus disease 2019 (COVID-19): situation report, 154". World Health Organization).

Wrapp, D., Wang, N., Corbett, K.S., Goldsmith, J.A., Hsieh, C.L., Abiona, O., Graham, B.S., and Mclellan, J.S. (2020). Cryo-EM structure of the 2019-nCoV spike in the prefusion conformation. *Science* 367, 1260-1263.

Yao, X.H., Li, T.Y., He, Z.C., Ping, Y.F., Liu, H.W., Yu, S.C., Mou, H.M., Wang, L.H., Zhang, H.R., Fu, W.J., Luo, T., Liu, F., Guo, Q.N., Chen, C., Xiao, H.L., Guo, H.T., Lin, S., Xiang, D.F., Shi, Y., Pan, G.Q., Li, Q.R., Huang, X., Cui, Y., Liu, X.Z., Tang, W., Pan, P.F., Huang, X.Q., Ding, Y.Q., and Bian, X.W. (2020). [A pathological report of three COVID-19 cases by minimal invasive autopsies]. *Zhonghua Bing Li Xue Za Zhi* 49, 411-417.

Supplementary Information

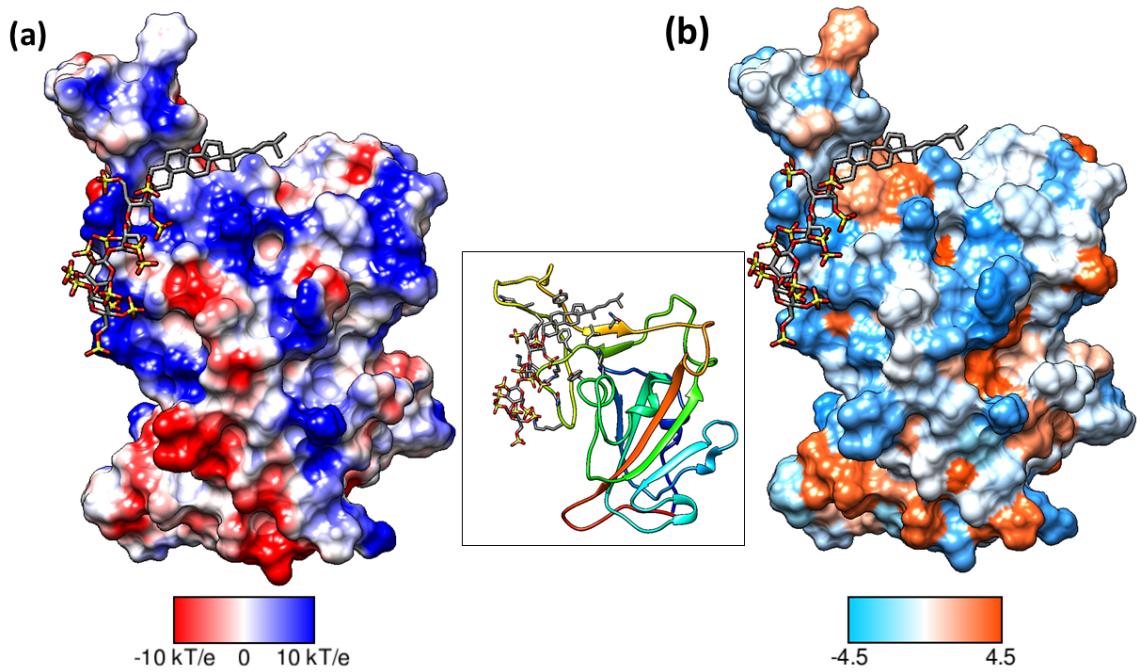

Figure S1. Binding mode of pixatimod on the S1 RBD (a) columbic surface and (b) hydrophobic surface. Both surfaces are oriented in the same direction as shown in the ribbon diagram of the protein in the middle. The sulfated tetrasaccharide interacts with the basic regions on S1 RBD whereas cholestanol residue prefers hydrophobic region for interactions. Coulombic surface coloring defaults: ε = 4r, thresholds ± 10 kcal/mol·e were used. Blue indicates surface with basic region whereas red indicates negatively charged surface. The hydrophobic surface was coloured using the Kyte-Doolittle scale wherein blue, white and orange red colour indicates most hydrophilicity, neutral and hydrophobic region, respectively. UCSF Chimera was used for creating surfaces and rendering the images. Hydrogens are not shown for clarity.

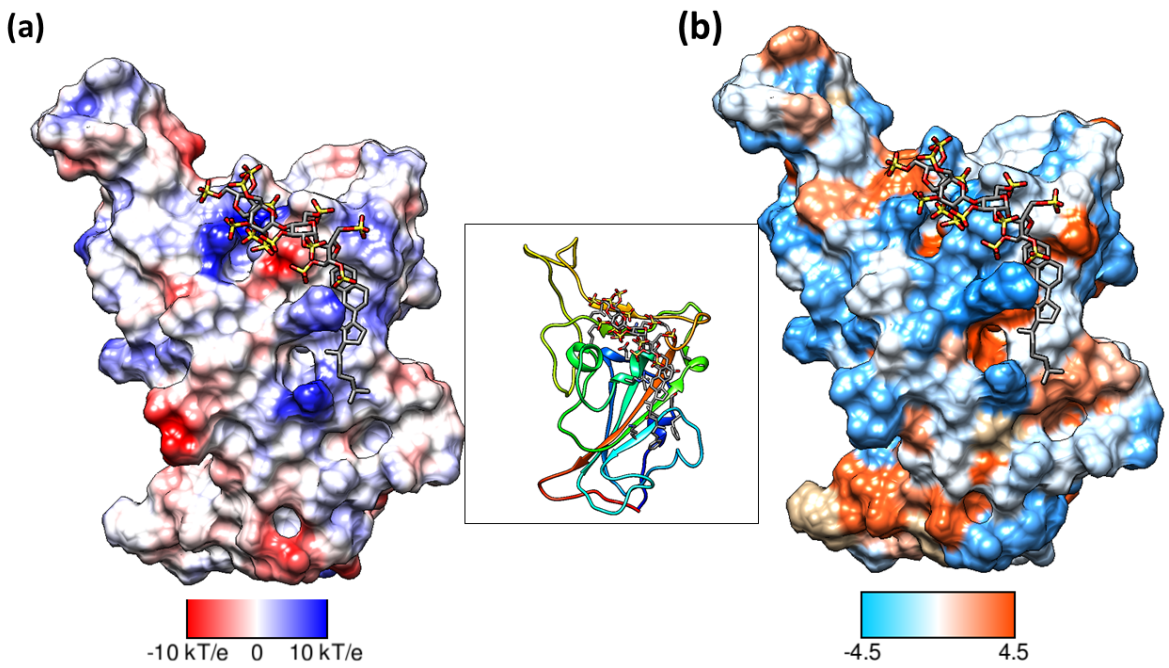

Figure S2. An alternate binding mode of pixatimod on the S1 RBD presented an unfavourable total binding free energy. Surfaces are oriented in the same direction as shown in the ribbon diagram in the inset. (a) Coulombic Surface Coloring defaults: ε = 4r, thresholds ± 10 kcal/mol·e were used. Blue indicates surface with basic region whereas red indicates negatively charged surface. (b) The hydrophobic surface was coloured using the Kyte-Doolittle scale wherein blue, white and orange red colour indicates most hydrophilic, neutral and hydrophobic region, respectively. UCSF Chimera was used for creating surfaces and rendering the images. Hydrogens are not shown for clarity.

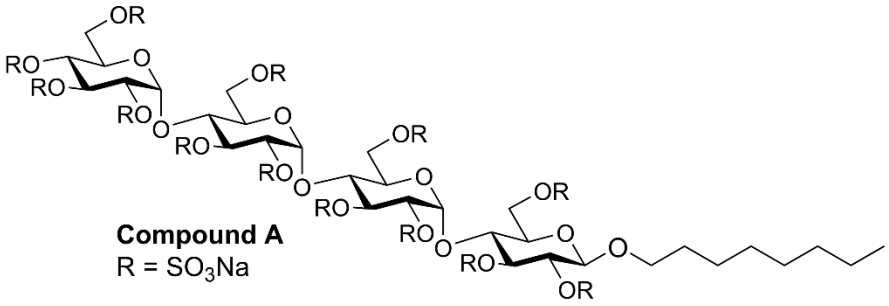

Figure S3. Structure of "control" compound A, octyl β-maltotetraoside tridecasulfate, an analogue of pixatimod without the steroid side chain.

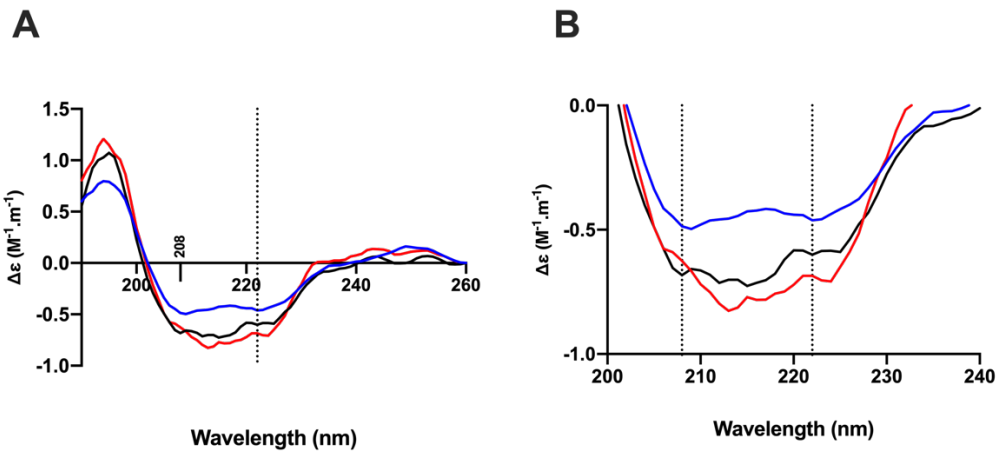

Figure S4: The conformational change of the SARS-CoV-2 S1 RBD observed in the presence of pixatimod by circular dichroism (CD) spectroscopy. (A). Circular dichroism spectra (190 - 260 nm) of SARS-CoV-2 S1 RBD alone (black solid line) and pixatimod (blue solid line) in PBS, pH 7.4. The red line represents the sum of the two individual spectra. Vertical dotted line indicates 222 nm (B) Details of the same spectra expanded between 200 and 240 nm. Vertical dotted lines indicate 222 nm and 208 nm.